Metals and Materials International (2021) 27:2406–2415
https://doi.org/10.1007/s12540-020-00886-4

Tuning the Microstructure and Mechanical Properties of Cold Sprayed Equiatomic CoCrFeMnNi High-Entropy Alloy Coating Layer

Ji-Eun Ahn[1] · Young-Kyun Kim[1] · Sang-Hoon Yoon[2] · Kee-Ahn Lee[1]

Received: 30 July 2020 / Accepted: 20 September 2020 / Published online: 21 October 2020
© The Korean Institute of Metals and Materials 2020

Abstract

An equiatomic CoCrFeMnNi high entropy alloy (HEA) coating layer was prepared via a cold spray (CS) process. In order to control the microstructure and nano-indentation properties of the CS HEA, heat treatments were employed. CS HEA coating layer showed a heterogeneous microstructure where ultra-fine grains were formed at the particle interfaces, while coarse grains were formed inside the particles. Furthermore, deformation twins (DTs) were also formed inside the particles due to severe plastic deformation (SPD) in each particle generated during the CS deposition. For the 550 °C heat treatment (HT), fine Cr-rich precipitates were additionally formed at the grain boundary and particle boundary. By contrast, recrystallization occurred during 850 °C HT, while the size of the Cr-rich precipitate increased. The nano-indentation hardness of the CS HEA coating layer was 10.9 GPa, which was ~3 times higher than that of the conventional cast HEA. The superior hardness of the CS HEA might has been enabled due to the combination of the high dislocation density, DTs, and ultra-fine grains. Based on the results above, the strategy to control the microstructure and mechanical properties through HT of the equiatomic CoCrFeMnNi HEA coating layer prepared via the CS process has been discussed.

Keywords High-entropy alloy · Cold spray · Coatings · Microstructure · Nanoindentation · Heat treatment

1 Introduction

High entropy alloy (HEA) or compositionally complex alloy (CCA), with unique properties, is a mixture of at least 5 principal elements, unlike conventional alloys, and each element exists at the mole fraction of 5–35 at% [1–4]. In addition, the HEA is characterized as not forming an intermetallic compound owing to its high configurational entropy. In particular, the equiatomic CoCrFeMnNi HEA (referred to as cantor alloy), which has been firstly developed among HEAs, has received extensive attention in the past 10 years due to its excellent tensile strength-ductility combination at cryogenic temperatures, high fracture toughness and corrosion resistance; therefore, numerous studies have been conducted [5–12].

Recently, due to the excellent physical and chemical properties of cantor alloy, its application as a coating layer as well as a bulk material is emerging [13, 14, 17]. In this regard, the fabrication of CoCrFeMnNi HEA coating layer has been attempted through various thermal spray processes (e.g. high-velocity oxygen fuel spraying (HVOF), atmospheric plasma spraying (APS), and plasma spraying, laser cladding) [15–17]. However, the coating layers manufactured by traditional thermal spray processes can exhibit poor physical properties due to defect formation and phase transformation [15–18]. Therefore, a cold spray (CS) that can create a part product having high hardness with dense structure is newly considered in the fabrication of CoCrFeMnNi HEA coating layer.

CS is a solid-state process in which metal powders are stacked by causing plastic deformation at a relatively low temperature upon colliding the 1 ~ 50 μm powder at a supersonic speed. Traditional thermal spray processes can cause oxide formation and phase transformation when the powder is melted, so the characteristics of the initial

Electronic supplementary material The online version of this article (https://doi.org/10.1007/s12540-020-00886-4) contains supplementary material, which is available to authorized users.

✉ Kee-Ahn Lee
keeahn@inha.ac.kr

[1] Department of Materials Science and Engineering, Inha University, Incheon 22212, Republic of Korea

[2] Industrial Materials Research Group, Research Institute of Industrial Science and Technology, Pohang 37673, Republic of Korea

powder can be changed in the resultant coating layer [15, 17]. However, the CS process is implemented at low temperature, phase transformation does not occur. In the case of the face-centered cubic (FCC) based metal, which is easily deformed, a dense coating layer can be produced [19–21]. In addition, high hardness and strength can be achieved by causing severe plastic deformation (SPD) on each powder. Therefore, if HEA alloy is produced into a coating layer through the CS, the application of this alloy is expected to be expanded.

To date, research on the fabrication of HEA coating layer using CS is extremely limited. Recently, Yin et al. [22] have manufactured the CoCrFeMnNi HEA coating layer through the CS and have proposed the wear resistance of the coating layer. However, the correlation between the superior mechanical properties and microstructures occurring in the CS CoCrFeMnNi HEA did not be reported. On the other hands, for the CS metallic coating layer, the mechanical properties such as strength, hardness, and ductility can be controlled through post heat treatment. However, the changes in the properties of the CS CoCrFeMnNi HEA coating layer via varying heat treatments have not been conducted at all.

In the present study, the equiatomic CoCrFeMnNi HEA coating layer was prepared using the CS, and its microstructure, hardness, and nano-indentation properties were examined. Various heat treatments were applied on the coating layer to control the mechanical properties of the CS equiatomic CoCrFeMnNi HEA. In addition, the correlation among nano-indentation properties, microstructure, and heat treatment of the CS equiatomic CoCrFeMnNi HEA was discussed.

2 Experimental Procedures

Figure 1 shows the (a) shape, (b) size distribution, (c) EDS mapping and (d) electron backscatter diffraction-inverse pole figure (EBSD-IPF) mapping results of the equiatomic CoCrFeMnNi HEA powders used in this study. First, the powder before CS had a sphere shape, the average powder size was about 27.2 μm, and the average grain size in the powder was 3.03 μm. Further, all the elements inside the powder were identified to be an even distribution (Fig. 1c). The pre-alloyed equiatomic

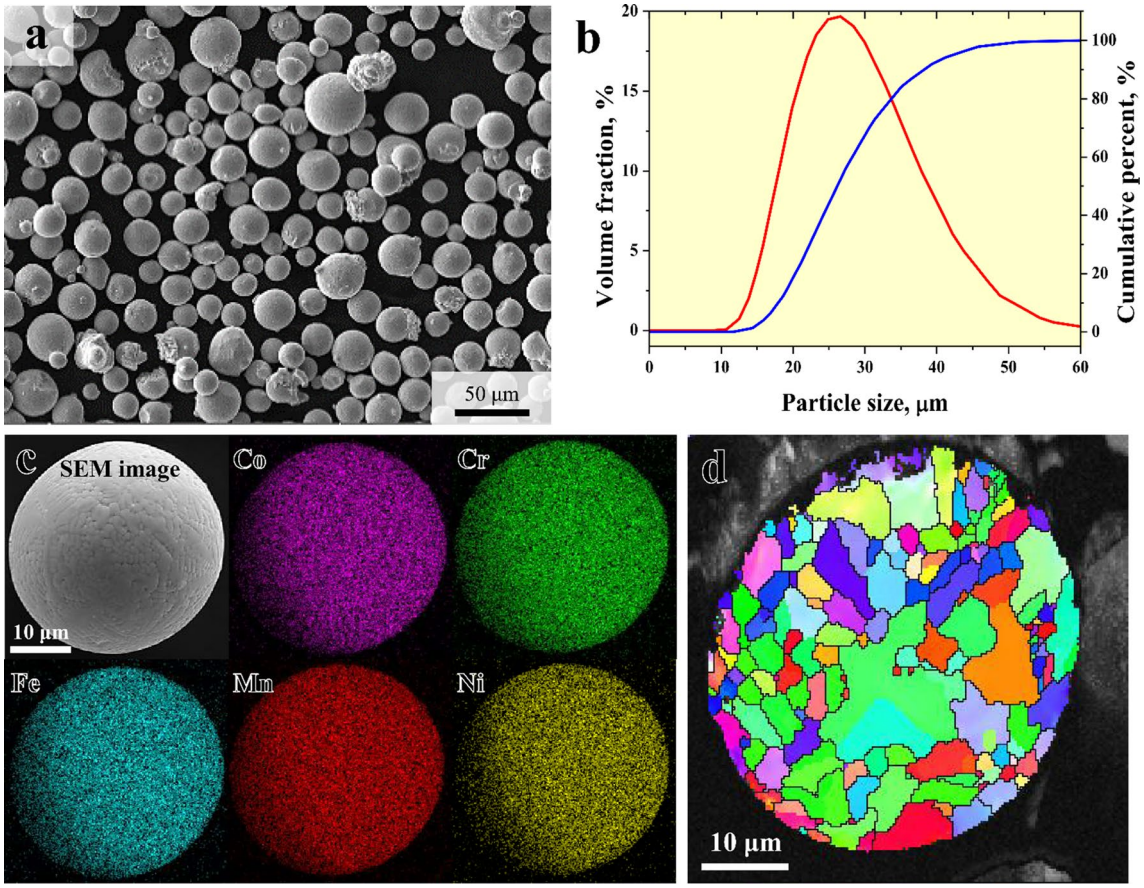

Fig. 1 **a** Morphology of initial equiatomic CoCrFeMnNi HEA powders observed by SEM, **b** distribution of powder size, **c** EDS mapping results of Co, Cr, Fe, Mn, and Ni elements, and **d** EBSD-IPF map image of equiatomic CoCrFeMnNi HEA powder

Table 1 Spray parameters for the manufacturing of CS equiatomic CoCrFeMnNi HEA

Spray parameters	
Gas	He
Pressure	3.0 MPa
Gas temperature	300 °C
Distance	30 mm
Traversal speed	100 mm/s
Powder pre-heating temperature	600 °C

CoCrFeMnNi HEA powders above were used as feedstock for CS processing. The CS was conducted on the low-alloy steel (substrate) and the process parameters arranged in Table 1. The Thickness of the deposited coating was measured to be 1 mm.

In order to change the microstructure and mechanical properties of the CS HEA coating layer, the heat treatments were induced at 550 °C and 850 °C under the Ar gas atmosphere for 2 hours each, followed by air cooling. A comparison material of bulk-type HEA (hereinafter referred as cast HEA) was also prepared with the vacuum induction casting to compare the microstructures and properties with the heat-treated (HT) HEA. The comparison material was prepared through the hot rolling after the casting and the heat treatment was conducted at 1000 °C for 24 h for homogenization. Meanwhile, the microstructures of the CS equiatomic CoCrFeMnNi HEA coating layer before and after the heat treatment were observed after the specimens were cut and polished with a silicon carbide paper and 1 µm diamond suspension, and then mirror polished with colloidal silica. Etching with the 50 ml H_2O + 50 ml HCl was followed to observe the microstructure. The microstructures of the etched samples were then examined by an optical microscope (OM, Olympus BX53M, Republic of Korea), a field-emission scanning electron microscopy (FE-SEM, TESCAN MIRA 3, Czech Republic), an electron backscatter diffraction (EBSD, Nordlys nano detector), and an electron channeling contrast imaging (ECCI). The step size during EBSD analysis was set to 130 nm.

The Vickers hardness of the coating layer was measured through a micro Vickers hardness tester (MATSUZAWA MMT-X7A, Japan) under the condition of the indentation load at 500 g and indentation time for 10 seconds. A nanoindentation (NANO-AIS, FRONTICS Inc., Republic of Korea) test was also performed to examine the local mechanical properties of the CS HEA coating layer with the indenter tip of Berkovich indenter under the condition of a maximum load at 20 mN and loading and unloading rates at 40 mN/min each at room temperature.

3 Results and Discussion

3.1 Microstructures of Cold Sprayed Coatings

Figure 2 shows the SEM micrographs (un-etched) of the as-sprayed HEA coating layer. The porosity of CoCrFeMnNi HEA was measured as 0.32%, indicating that the present HEA was soundly fabricated through the CS process. Furthermore, for the HEAs manufactured via thermal spray processes, it was confirmed that the fraction of defects was relatively larger than the present CS HEA, and phase transformation may occur in the conventional thermal-sprayed HEA coatings due to high-temperature energy [15–18]. By contrast, the CS process does not cause phase transformation and can maintain a single phase. Furthermore, the defect fraction was also lower than those in the thermal-sprayed HEAs. In addition, the interfaces of the particles were not prominent in the microstructure, which implied that the metallic bonding occurred in the CS deposition mechanisms. However, some pores or micro-cracks formed in the regions where the metallic bonding was not completed.

Figure 3 represents the OM micrographs of the CS HEA coating layers treated at 550 °C (a) and 850 °C (b) (hereinafter referred to as H550 and H850, respectively). After heat treatments at 550 °C and 850 °C, the porosity did not change significantly. However, the fine second phase particles, which were not observed in the as-sprayed HEA, could be found additionally along the specific areas of the particle interfaces and grain boundaries in the H550. For the H850, full recrystallization occurred, and re-distribution and coarsening of the second phase particles were found. Moreover, the deposited particles showed elongated shapes vertically toward the spraying direction.

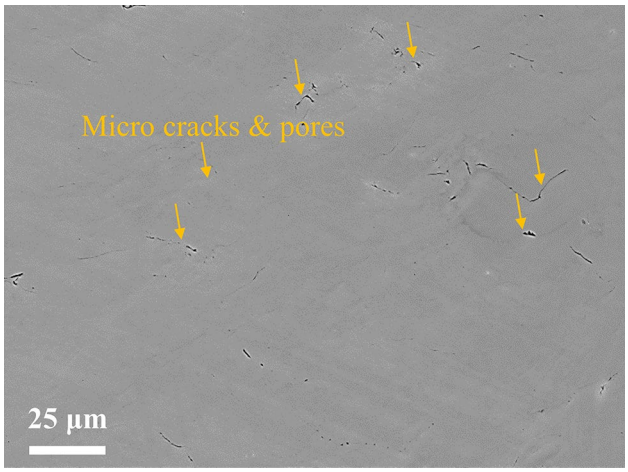

Fig. 2 SEM micrograph (un-etched) of as-sprayed equiatomic CoCrFeMnNi HEA coating layer

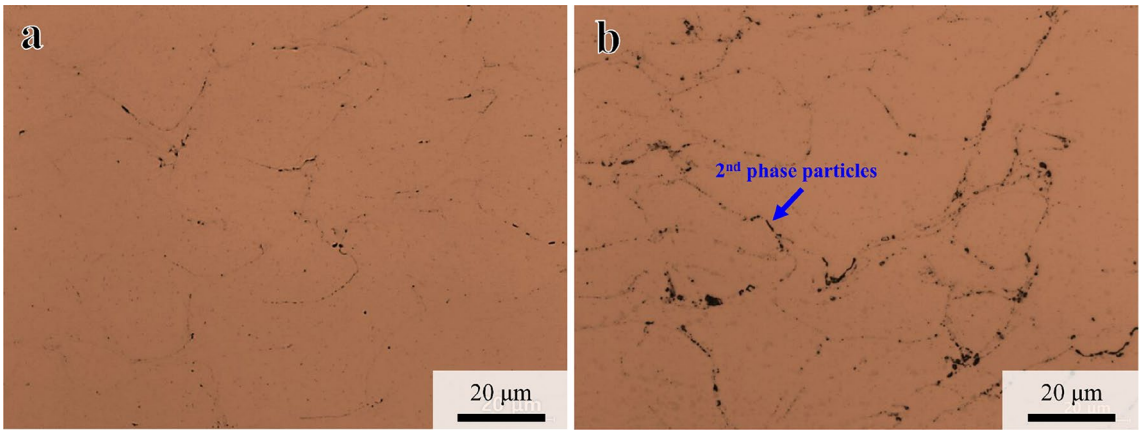

Fig. 3 Optical micrographs (un-etched) of cross sectional equiatomic CoCrFeMnNi HEA coating layers after heat treatments at **a** 550 ℃ and **b** 850 ℃ for 2 h

The etched microstructures of the CS HEA and HT HEA coating layers were observed through high-magnification SEM, and the results are presented in Fig. 4. In case of the as-sprayed HEA, the particle interfaces were clearly distinguished (Fig. 4a_1) unlike those before etching, which was a normal phenomenon in the CS metallic materials. It was because, in the case of the particle interface, some regions were metallically bonded or mechanically locked, rendering it unstable compared to its interior. In other words, harsher deformation was concentrated in the particle interface, which made the unstable state [23]. Also, deformation twins (DTs) that are known to improve mechanical properties were observed in the enlarged image (Fig. 4a_2). The magnified ECC image revealed that in the DTs, nano twins of ~20 nm formed bundles in particle interior than the particle interface (Fig. S1). Formation of DTs in the CS process

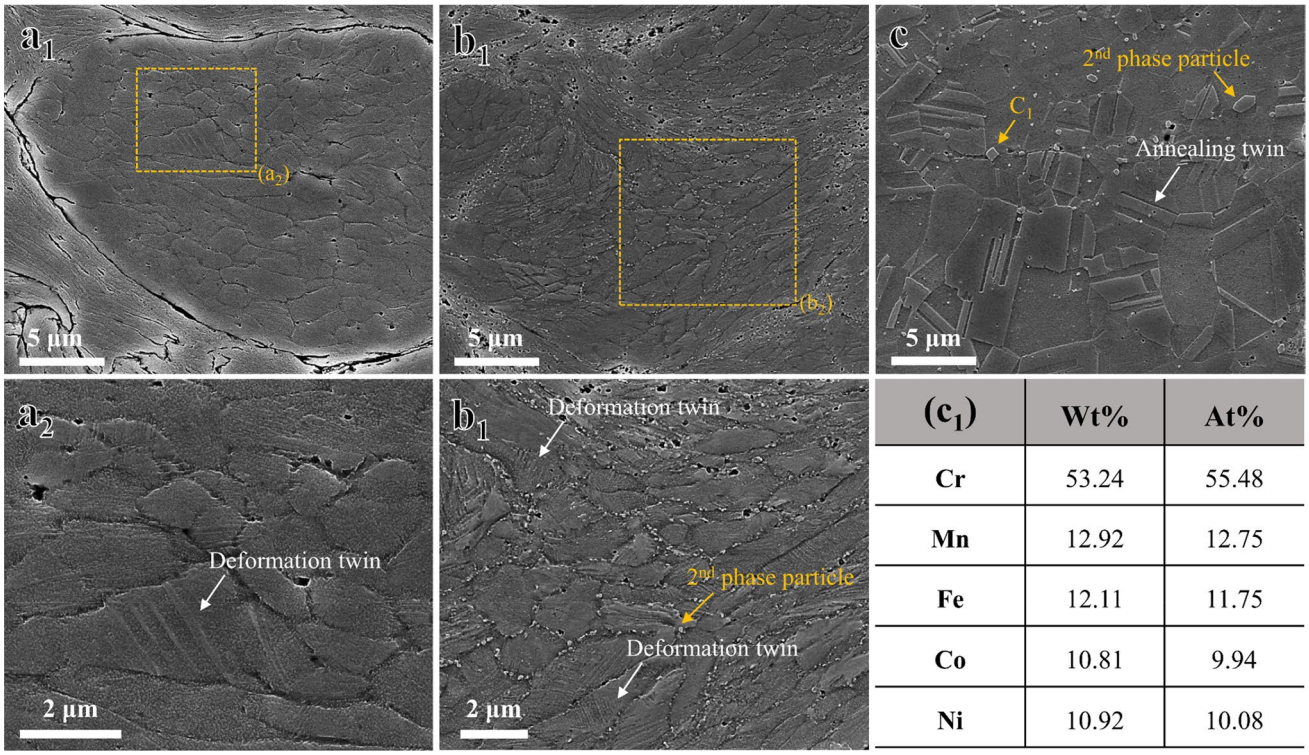

(c_1)	Wt%	At%
Cr	53.24	55.48
Mn	12.92	12.75
Fe	12.11	11.75
Co	10.81	9.94
Ni	10.92	10.08

Fig. 4 SEM micrographs (etched) of equiatomic CoCrFeMnNi HEA coating layers: $\mathbf{a_1}$, $\mathbf{a_2}$ as-sprayed HEA, $\mathbf{b_1}$, $\mathbf{b_2}$ H550, **c** H850, and $\mathbf{C_1}$ EDS point analysis results

has been reported in Cu [24] and Ni [19, 25] to date. In case of the Cu and Ni, formation of the nano-twins in the particle interface, where a large strain accumulation occurred, has been reported. Here, the DT, which was generated during the strain accumulation, was affected by the intrinsic (grain size and stacking fault energy (SFE)) and external (strain) parameters [26]. Here, the critical stress for twinning can be calculated through the intrinsic parameters and Eq. (1) [6].

$$\sigma_T = M\frac{\gamma}{b_p} + \frac{k_T}{\sqrt{d}} \tag{1}$$

where, σ_T is critical stress for twinning stress, M is the Taylor factor, γ represents SFE, b_p denotes Burgers vector of a partial dislocation, k_T denotes the Hall-Petch constant for twinning, and d is the average grain size. In other words, DTs can be easily formed as SFE decreased. In general, SFE is an important parameter determining the deformation twins in FCC-structured metals and austenitic stainless steel [27–30]. It is also well known that a large amount of nano-twins could be formed at particle interfaces during a CS process in the medium SFE metals (Cu: -78 mJ/m^2 [24], Ni: -130 mJ/m^2 [25]). These suggest that the CoCrFeMnNi HEA, which has low SFE of ~21 mJ/m^2 [31, 32], can induce deformation twinning more easily during a CS process. Herein, the formation of DT can act as an additional strengthening factor in CS HEA because the DT can suppress the dislocation motion, and reduce the dislocation mean free path [33].Considering the above results, since equiatomic CoCrFeMnNi HEA has low SFE (~21 mJ/m^2), it is expected that nano-twins could be easily generated inside the particle during CS, which contribute to the excellent strength and hardness of CS HEA.

On the other hand, H550 coating layer showed that the DTs were still presented even after the heat treatment (Fig. 4b$_{1-2}$). Further, the second phases having a size of ~200 nm, which were not observed in the as-sprayed HEA coating layer, were precipitated in the particle interface and grain boundary. This results well accord to the OM images of the H500 coating layer (Fig. 3). Meanwhile, the microstructure of the H850 coating layer showed that the full recrystallization occurred, and a significant quantity of annealing twins were also formed along with the precipitates of size about 1 μm at the grain boundary and twin boundary. EDS point analysis results confirmed that the second phases formed in the HT samples were the Cr-rich precipitates. The fractions of the second phase particles of H550 and H850 were obtained as 1.6 ± 0.17% and 1.7 ± 0.17% from the SEM image-based analysis, indicating that the difference in fraction was not significant. However, the average precipitate's size of the two HT HEA coatings was measured as 200 nm (H550) and 1 μm (H850), respectively, implying that the size tended to increase with increase in the heat-treatment temperature. This means that, in the H550, microstructural characteristics of the as-sprayed HEA were maintained and some precipitates were formed. In addition, the second phase particles formed preferentially in the order: particle boundary > grain boundary > twin boundary.

Figure 5 shows the EDS elemental distribution maps corresponding to the SEM images depending on the heat-treatment temperatures. In the as-sprayed HEA, Co, Cr, Fe, Mn, and Ni elements were evenly distributed without the segregation of the specific element (Fig. 5a). In case of the H550, segregation of specific elements did not occur even after the heat treatment, and all the elements were evenly distributed (Fig. 5b). However, the second phases of size ~200 nm, as shown in Fig. 4b$_{1-2}$, were not found in the EDS mapping results, which might be because of their small sizes, thus enabling them to not be detected through the EDS. In case of the H850 coating layer, which was full recrystallized, the Cr-rich precipitates about 1 μm were formed as shown in Fig. 4c. The Cr-rich phases was assumed to be the σ phase which was mainly formed during the heat treatment of the equiatomic CoCrFeMnNi HEA coating layer. In general, the σ phase in the equiatomic CoCrFeMnNi HEA was a non-magnetic, topologically closed-packed (TCP) phase having a tetragonal structure (space group $P4_2/mnm$) and known to be formed in the temperature zone of 600–1000 °C [34–37]. This phase had a composition in the range of XY_7 to X_7Y, and X was an IUPAC group 3–6 element same as Cr, while Y was Co, Fe, Mn, and Ni, which was 7–10 element. In addition, when the CoCrFeMnNi HEA had a coarse grain size, it took mostly tens to hundreds of days to precipitate the σ phase [37]. Unlike this, the σ phase can be precipitated even with the few minutes of heat treatment when HEA had initially nanocrystalline grain sizes [37–39]. The σ phase could be dependent on the initial microstructure. In case of the HEA, σ phase was formed even with the heat treatment at 550 °C for 2 hours since high strain imposed though the alloy doesn't have nanocrystalline grain size. Generally, σ phase is brittle intermetallic compounds and can deteriorate mechanical properties. Therefore, the coarsening of σ phase should be strictly controlled. However, if the heat treatment condition is appropriately controlled, fine σ phases can increase both strength and strain hardening. Furthermore, it may induce additional grain refinement effect due to grain boundary pinning [40, 41].

Figure 6 shows the EBSD analysis results of the as-sprayed HEA, H550, H850 HEA coating layers, and cast HEA (reference material). In case of the as-sprayed HEA, the grains of some hundreds of nm in size were found at the particle interface (Fig. 6a). In addition to this, large quantity regions which could not be detected in the EBSD analysis were found around the particle interfaces. This indicates that CS induced severe lattice distortion at the particle interfaces. Nonetheless, though significant changes in grain

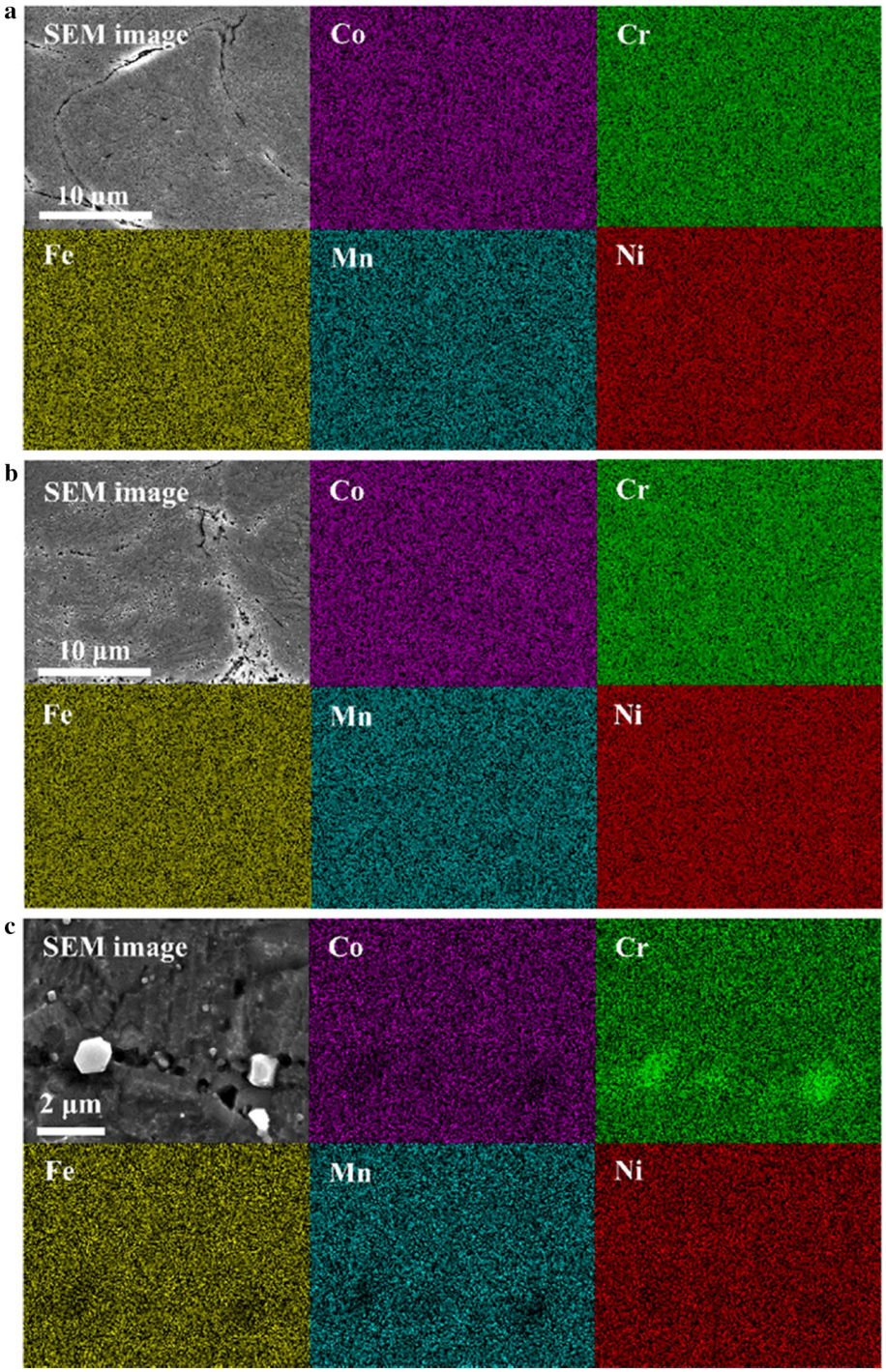

Fig. 5 EDS mapping images of Co, Cr, Fe, Mn, and Ni element of equiatomic CoCrFeMnNi HEA coating layers: **a** as-sprayed HEA, **b** H550, and **c** H850

size were not found in H550 as compared to the as-sprayed HEA, the detected regions were largely increased (Fig. 6b). This can be understandable owing to the recovery phenomenon occurring during the heat-treatment at 550 °C. H850 sample, which recrystallization occurred as can be seen in the SEM image, revealed the recrystallized grains having random crystallographic orientation. The average grain size of the H850 coating layer was measured as 2.35 µm and large number density of annealing twins were also observed (Fig. 6c). Whereas, cast HEA presents relatively coarse grains (~243 µm) than H850 sample (Fig. 6d).

It has been reported that in the case of the CS metallic materials, a large quantity of dynamic recrystallized (DRXed) grains could be formed in the particle interface. Kim et al. [42] reported that CS Cu shows bi-modal structures, which had relatively coarse grains and ultra-fine grains, due to severe strain difference between the particle interface and interior. Generally, it is known that when the

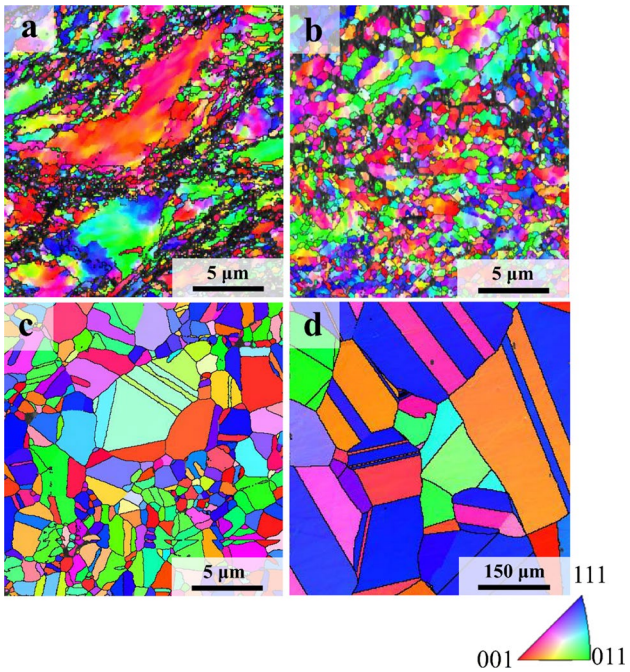

Fig. 6 EBSD IPF maps of equiatomic CoCrFeMnNi HEA coating layers: **a** as-sprayed HEA, **b** H550, **c** H850, and **d** cast HEA

powder was deposited on the matrix by supersonic speed during a CS process, the heat concentrated regions could be formed due to SPD, and this called thermal boost-up zone (TBZ). Such TBZ and rapid plastic deformation resulted to an adiabatic shear instability (ASI), which was thermally unstable and where consequently DRX was generated [42]. These DRXed grains have been known to improve mechanical properties. Since a large quantity of DRXed grains were formed in the CS HEA, its excellent mechanical properties are expected.

3.2 Vickers and Nano-indentation Hardness Results

The Vickers hardness values of the as-sprayed HEA and HT HEA coating layers were measured, and the results are shown in Fig. 7. The as-sprayed HEA, H550, H850 and cast HEA had the hardness values of 423.8, 399.6, 219.9, and 143.9 HV, respectively. This means that CS HEA revealed higher hardness by 2.94 times compared to the cast HEA. Also, when comparing to the other HEA having excellent mechanical properties such as additively manufactured HEA (AM-built HEA) and Nb-C reinforced HEA, CS HEA revealed relatively higher hardness level [43, 44]. In particular, when compared with the equiatomic CoCrFeMnNi HEA prepared by the SPD process (e.g., high pressure torsion (HPT)) known to have high hardness, the hardness of the CS HEA was similar to that of 1 turn material of the HPT HEA, and lower than 5 turns material [45]. On the other hand,

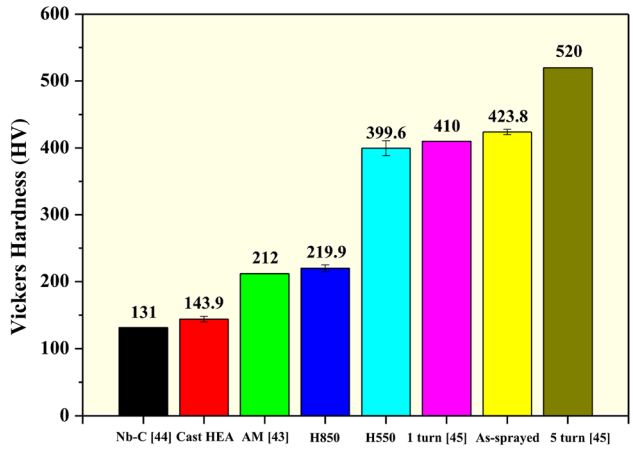

Fig. 7 Vickers hardness results of equiatomic CoCrFeMnNi HEA materials [43–45]

for the H550 coating layer, the hardness was still superior though the hardness was somehow reduced due to recovery, as observed in the EBSD IPF map (Fig. 6b). It might be because the nano scale σ phases formation acted as reinforcing particles even if there was a recovery [40, 41]. Similarly, though the H850 coating layer had full recrystallized grains, the hardness was superior than the cast HEA and similar to that of the AM-built HEA. This suggests that the DRXed fine grains in the CS and HT coating layers enabled higher mechanical property compared to cast HEA.

The notable point in the hardness properties was that the deviation of the hardness of the CS HEA coating layer was significantly small. In the case of the CS metallic coating material, in general, the mechanical properties are significantly different between the interior and interface of the particle due to DRXed grains formed in the particle interface [42]. However, there was no significant hardness difference between the interior and interface of the particles in the case of the CS HEA coating layer, which might be due to high number density of DTs observed in the ECC images (please see the Fig. S1). Cu and Ni, which had the medium stacking fault energy (SFE), formed nano-twins along with the DRX at the particle interface, but DTs were almost not formed inside the particle. On the other hand, abundant nano-twins could be formed even inside the particle, along with the interface, since the equiatomic CoCrFeMnNi HEA coating layer had a low SFE [46, 47]. Therefore, similar hardness could be obtained in the particle interface and interior in this study.

Figure 8 presents the nano-indentation load-penetration depth (*P*-*h*) curves of the HEA coating layers. Here, the nano-indentation was conducted for the as-sprayed HEA, H550, H850, and cast HEA. The *P*-*h* curves show that the indenter displacement as against the indentation load was in the order of the as-sprayed HEA < H550 < H850 < cast

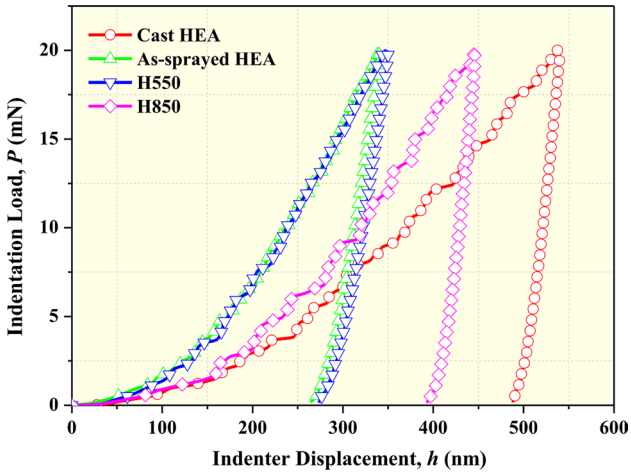

Fig. 8 Load-displacement curves obtained from nanoindentation tests of equiatomic CoCrFeMnNi HEA materials

HEA. This indicates that the as-sprayed HEA and the H550 showed similar indentation behaviors and corresponds well with the hardness difference tendency as shown in Fig. 7. In case of the H850, it had relatively small grains compared to the cast HEA, and the indenter displacement exhibited low levels.

The indentation hardness (H_{IT}) and elastic modulus (E_{IT}) values were determined from the *P–h* curve according to the Oliver–Pharr (O-P) method and the results are shown in Fig. 9 [48]. In case of the as-sprayed HEA, the indentation hardness was also excellent compared to the cast HEA, and its properties were maintained in the H550 (Fig. 9a). The elastic modulus was also well-matched with the above results. In case of the H850, the deviation of the elastic modulus was considerably large, which might be the effect of the σ phases of a size about 1 μm, formed after the heat treatment. The CS HEA showed the superior mechanical properties, which might be due to the DTs formed inside the particle in a large quantity, as well as the high dislocation density, which was the characteristic of the CS metallic materials. Furthermore, the H550 could be expected to improve the low ductility and toughness, which were drawbacks of the CS metallic materials, by inducing the microstructural recovery, while not significantly impairing the hardness.

The mechanical properties such as H_{IT}, E_{IT}, H_{IT}/E_{IT}, H_{IT}^3/E_{IT}^2 and $1/E_{IT}^2H_{IT}$ of CS HEA were calculated and shown in Table 2. Here, H_{IT}/E_{IT}, H_{IT}^3/E_{IT}^2 and $1/E_{IT}^2H_{IT}$ represent wear resistance, ability to resist plastic deformation, and resistance to crack damage, respectively [49–52]. The resistances to wear and plastic deformation of as-sprayed HEA are significantly higher than cast HEA. After heat treatment at 550 °C, the resistance to wear and plastic deformation slightly decreased (0.015 to 0.013), but the ability to resist crack damage increased significantly (1.057 to 1.251). This implies that heat treatment at 550 °C could improve the resistance to crack damage while also maintaining resistance to wear and plastic deformation.

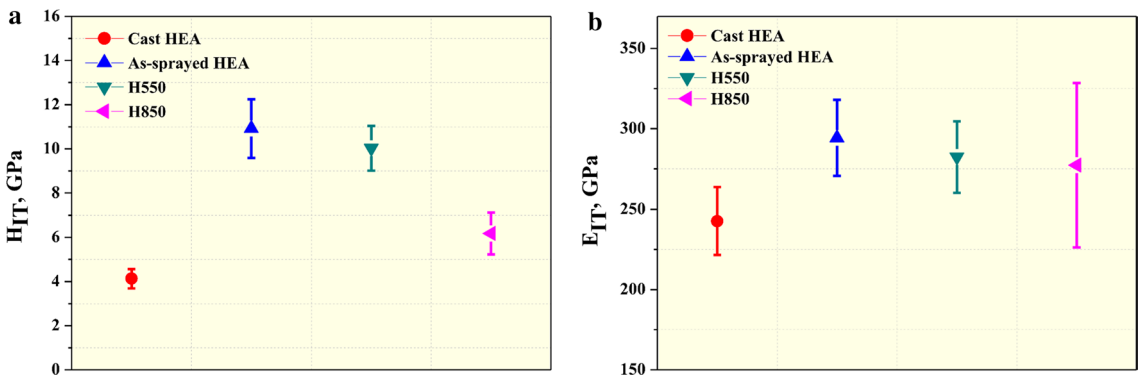

Fig. 9 **a** Indentation hardness and **b** elastic modulus results obtained from nanoindentation tests of equiatomic CoCrFeMnNi HEA materials

Table 2 Mechanical properties of CSed equiatomic CoCrFeMnNi HEA

	H_{IT} (GPa)	E_{IT} (GPa)	H_{IT}/E_{IT}	H_{IT}^3/E_{IT}^2 (GPa)	$1/E_{IT}^2H_{IT}$ (GPa^{-3}) × 10^6
Cast HEA	4.13 ± 0.44	242.63 ± 21.04	0.017	0.0012	4.112
As-sprayed HEA	10.92 ± 1.33	294.32 ± 23.64	0.037	0.015	1.057
H550	10.02 ± 1.02	282.34 ± 22.30	0.036	0.013	1.251
H850	6.18 ± 0.95	277.35 ± 51.22	0.022	0.003	2.105

4 Conclusions

In this study, an equiatomic CoCrFeMnNi HEA was prepared through the CS process and the effect of the heat treatment on the microstructures and nanoindentation properties were examined. The obtained results are as follows.

(1) The CS HEA coating layer showed a heterogeneous microstructure in which ultra-fine grains were formed in the particle interface, while coarse grains were formed in the particle interior. In addition, large number density of DTs was formed in the particle interior of the as-sprayed HEA and the H550 coating layers. Meanwhile, the H850 coating layer was full recrystallized and the grains with an average of 2.35 μm were found. In addition to this, when comparing the grain sizes to the cast HEA, as-sprayed- and HT HEA coating layers revealed relatively fine grain sizes.

(2) After the heat treatment, the Cr-rich precipitate σ phases were formed in both the H550 and H850 coating layers. In case of the H550, the σ phases were formed at the particle interfaces and grain boundaries, while in case of the H850, the σ phases with a size of about 1 μm were observed at both grain boundaries and annealing twin boundaries.

(3) The hardness of the as-sprayed HEA was measured 423.8 HV, which was higher by about 3 times as compared with the cast HEA with a hardness value of 143.9 HV. The excellent mechanical properties of the CS equiatomic CoCrFeMnNi HEA might be attributed to the combination of the ultra-fine grains in the particle interface, interior DTs, and high dislocation density. The hardness of the H550 and H850 coating layers were 399.6 HV and 219.9 HV, respectively, exhibiting superior mechanical properties even after the heat treatment compared to that of the cast HEA.

(4) The nanoindentation test results showed that the indenter displacement was in the order of the as-sprayed HEA < H550 < H850 < cast HEA. The nanoindentation hardness of the as-sprayed HEA was measured ~ 10.9 GPa and was maintained even after the heat treatment at 550 °C. Although the recovery occurred in the HT coating layer, superior Vickers and nanoindentation hardness were obtained, which could be explained by the formation of the nanoscale σ phases. Excellent resistance to wear and plastic deformation was also maintained after 550 °C heat treatment, and the resistance to crack damage was improved compared to as-sprayed HEA.

Acknowledgements This study was supported by Korea Institute for Advancement of Technology (KIAT) grant funded by the Korea Government (MOTIE) (P0002007, The Competency Development Program for Industry Specialist). It was also supported by National Research Foundation of Korea (NRF) grant funded by the Korea government (MEST) (No. 2019R1A2C1008904).

References

1. D.B. Miracle, O.N. Senkov, Acta Mater. **122**, 448 (2017)
2. B. Cantor, I.T.H. Chang, P. Knight, A.J.B. Vincent, Mater. Sci. Eng. A **375**, 213 (2004)
3. J.-W. Yeh, S.-K. Chen, S.-J. Lin, J.-Y. Gan, T.-S. Chin, T.-T. Shun, C.-H. Tsau, S.-Y. Chang, Adv. Eng. Mater. **6**, 299 (2004)
4. B. Cantor, Entropy **16**, 4749 (2014)
5. Y.-K. Kim, Y.-A. Joo, H.S. Kim, K.-A. Lee, Intermetallics **98**, 45 (2018)
6. Y.-K. Kim, G.-S. Ham, H.S. Kim, K.-A. Lee, Intermetallics **111**, 106486 (2019)
7. B. Gludovatz, A. Hohenwarter, D. Catoor, E.H. Chang, E.P. George, R.O. Ritcie, Science **345**, 1153 (2014)
8. Y. Lu, X. Gao, L. Jiang, Z. Chen, T. Wang, J. Jie, H. Kang, Y. Zhang, S. Guo, H. Ruan, Y. Zhao, Z. Cao, T. Li, Acta Mater. **124**, 143 (2017)
9. M. Kang, J.W. Won, K.R. Lim, S.H. Park, S.M. Seo, Y.S. Na, Korean J. Met. Mater. **55**, 732 (2017)
10. E. Colombini, R. Rosa, L. Trombi, M. Zadra, A. Casagrande, P. Veronesi, Mater. Chem. Phys. **210**, 78 (2018)
11. M.L. Brocq, P.-A. Goujon, J. Monnier, B. Villeroy, L. Perrire, R. Pirs, G. Garchin, J. Alloys Compd. **780**, 856 (2019)
12. Y.-K. Kim, J. Choe, K.-A. Lee, J. Alloys Compd. **805**, 680 (2019)
13. Q. Ye, K. Feng, Z. Li, F. Lu, R. Li, J. Huang, Y. Wu, *Appl. Surf. Sci.* **396**, 1420 (2017)
14. M.Z. Ghomsheh, G. Khatibi, B. Weiss, M. Lederer, S. Schwarz, A.S. -T, M.A. Tikhonovsky, E.D. Tabachnikova, E. Schafler, Mater. Sci. Eng. A **777**, 139034 (2020)
15. W.-L. Hsu, H. Murakami, J.-W. Yeh, A.-C. Yeh, K. Shimoda, Surf. Coat. Technol. **316**, 71 (2017)
16. L. Chen, K. Bobzin, Z. Zhou, L. Zhao, M. Öte, T. Königstein, Z. Tan, D. He, Surf. Coat. Technol. **358**, 215 (2019)
17. J.-K. Xiao, H. Tan, Y.-Q. Wu, J. Chen, C. Zhang, Surf. Coat. Technol. **385**, 125430 (2020)
18. F. Chang, B. Cai, C. Zhang, B. Huang, S. Li, P. Dai, Surf. Coat. Technol. **359**, 132 (2019)
19. C. Lee, J. Kim, J. Therm. Spray Technol. **24**, 592 (2015)
20. H.-J. Kim, C.-H. Lee, S.-Y. Hwang, Surf. Coat. Technol. **191**, 335 (2005)
21. A.P. Alkhimov, A.N. Papyrin, V.F. Kosarev, N.I. Nesterovich, M.M. Shushpanov, Gas-dynamic spraying method for applying a coating, U.S. Patent 5,302,414, 12 Apr 1994
22. S. Yin, W. Li, B. Song, X. Yan, M. Kuang, Y. Xu, K. Wen, R. Lupoi, J. Mater. Sci. Technol. **35**, 1003 (2019)
23. R. Partovi-Nia, S. Ramamurthy, D. Zagidulin, J. Chen, R. Jacklin, P. Keech, D. Shoesmith, Corrosion **71**, 1237 (2015)
24. Y. Zhang, N. Brodusch, S. Descartes, R. Chromik, R. Gauvin, Microsc. Microanal. **20**, 1499 (2014)
25. G. Bae, K. Kang, C. Lee, Mater. Lett. **89**, 320 (2012)
26. Y. Deng, C.C. Tasan, K.G. Pradeep, H. Springer, A. Kostka, D. Raabe, Acta Mater. **94**, 124 (2015)
27. D. Wei, X. Li, J. Jiang, W. Heng, Y. Koizumi, W.-M. Choi, B.-J. Lee, H.S. Kim, H. K, A. Chiba, Scr. Mater. **165**, 39 (2019)
28. D. Wei, X. Li, S. Schönecker, J. Jiang, W.-M. Choi, B.-J. Lee, H.S. Kim, A. Chiba, H. Kato, Acta Mater. **181**, 318 (2019)
29. T.-H. Lee, E. Shin, C.-S. Oh, H.-Y. Ha, S.-J. Kim, Acta Mater. **58**, 3173 (2010)

30. J. Lu, L. Hultman, E. Holmström, K.H. Antonsson, M. Grehk, W. Li, L. Vitos, A. Golpayegani, Acta Mater. **111**, 39 (2016)
31. G. Laplanche, A. Kostka, O.M. Horst, G. Eggeler, E.P. George, Acta Mater. **118**, 152 (2016)
32. S.F. Liu, Y. Wu, H.T. Wang, J.Y. He, J.B. Liu, C.X. Chen, X.J. Liu, H. Wang, Z.P. Lu, Intermetallics **93**, 269 (2018)
33. F. Otto, A. Dlouhý, Ch Somsen, H. Bei, G. Eggler, E.P. George, Acta Mater. **61**, 5743 (2013)
34. G. Laplanche, S. Berglund, C. Reinhart, A. Kostka, F. Fox, E.P. George, Acta Mater. **161**, 338 (2018)
35. M.-H. Tsai, K.-C. Chang, J.-H. Li, R.-C. Tsai, A.-H. Cheng, Mater. Res. Lett. **4**, 90 (2016)
36. M.-H. Tsai, K.-Y. Tsai, C.-W. Tsai, C. Lee, C.-C. Juan, J.-W. Yeh, Mater. Res. Lett. **1**, 207 (2013)
37. F. Otto, A. Dlouhý, K.G. Pradeep, M. Kuběnová, D. Raabe, G. Eggeler, E.P. George, Acta Mater. **112**, 40 (2016)
38. B. Schuh, F. Mendez-Martin, B. Völker, E.P. George, H. Clemens, R. Pippan, A. Hohenwarter, Acta Mater. **96**, 258 (2015)
39. H. Shahmir, J. He, Z. Lu, M. Kawasaki, T.G. Langdon, Mater. Sci. Eng. A **676**, 294 (2016)
40. Y.H. Jo, W.M. Choi, D.G. Kim, A. Zargaran, K. Lee, H. Sung, S.S. Sohn, H.S. Kim, B.J. Lee, S. Lee, Mater. Sci. Eng. A **743**, 665 (2019)
41. Y.H. Jo, W.-M. Choi, S.S. Sohn, H.S. Kim, B.-J. Lee, S. Lee, Mater. Sci. Eng. A **724**, 403 (2018)
42. Y.-K. Kim, K.-S. Kim, H.-J. Kim, C.-H. Park, K.-A. Lee, J. Therm. Spray Technol. **26**, 1498 (2017)
43. A. Piglione, B. Dovgyy, C. Liu, C.M. Gourlay, P.A. Hooper, M.S. Pham, Mater. Lett. **224**, 22 (2018)
44. E. Abbasi, K. Dehghani, Mater. Sci. Eng. A **753**, 224 (2019)
45. B. Schuh, F. Mendez-Martin, B. Völker, E.P. George, H. Clemens, R. Pippan, A. Hohenwarter, Mechanical properties. Acta Mater. **96**, 258 (2015)
46. S. Huang, W. Li, S. Lu, F. Tian, J. Shen, E. Holmström, L. Vitos, Scr. Mater. **108**, 44 (2015)
47. P.-L. Sun, Y.H. Zhao, J.C. Cooley, M.E. Kassner, Z. Horita, T.G. Langdon, E.J. Lavernia, Y.T. Zhu, Mater. Sci. Eng. A **525**, 83 (2009)
48. W.C. Oliver, G.M. Pharr, Mat. Res. **19**, 3 (2004)
49. C. Sha, Z. Zhou, Z. Xie, P. Munroe, Surf. Coat. Technol. **385**, 125435 (2020)
50. A. Leyland, A. Mattews, Wear **246**, 1 (2000)
51. M. Roy, L. Whiteside, J. Xu, B. Katerberg, Acta Biomater. **6**, 1619 (2010)
52. A. Miserez, J.C. Weaver, P.J. Thurner, J. Aizenberg, Y. Dauphin, P. Fratzl, D.E. Morse, F.W. Zok, Adv. Funct. Mater. **18**, 1241 (2008)

Publisher's Note Springer Nature remains neutral with regard to jurisdictional claims in published maps and institutional affiliations.